Mission Applications of a HIAD for the Mars Southern Highlands

Richard Winski
Binera, Inc.
203 Colleen Drive
Yorktown, VA 23693
757-864-4116
richard.g.winski@nasa.gov

Dave Bose
Analytical Mechanics Associates, Inc.
2101 NASA Parkway
Hampton, VA
281-483-8223
dmbose@ama-inc.com

David R. Komar
NASA Langley Research Center
MS 451
Hampton, VA 23681
757-864-9355
d.r.komar@nasa.gov

Jamshid Samareh
NASA Langley Research Center
MS 451
Hampton, VA 23681
757-864-5776
jamshid.a.samareh@nasa.gov

***Abstract*—Recent discoveries of evidence of a flowing liquid in craters throughout the Mars Southern Highlands, like Terra Sirenum, have spurred interest in sending science missions to those locations; however, these locations are at elevations that are much higher (0 to +4 km MOLA) than any previous landing site (-1 to -4 km MOLA). New technologies may be needed to achieve a landing at these sites with significant payload mass to the surface. A promising technology is the hypersonic inflatable aerodynamic decelerator (HIAD); a number of designs have been advanced but the stacked torus has been recently successfully flight tested in the IRVE-2 and IRVE-3 projects through the NASA Langley Research Center. This paper will focus on a variety of mission applications of the stacked torus type attached HIAD to the Mars southern highlands.**

TABLE OF CONTENTS

1. INTRODUCTION

Recent discoveries of evidence of a flowing liquid in craters throughout the Mars Southern Highlands, like Terra Sirenum[1], have spurred interest in sending science missions to those locations; however, these locations are at elevations that are much higher (0 to +4 km MOLA) than any previous landing site (-1 to -4 km MOLA)(Fig. 1). New technologies may be needed to achieve a successful landing at these sites with adequate payload mass to the surface. A promising technology is the hypersonic inflatable aerodynamic decelerator (HIAD); a number of designs have been advanced and the stacked torus has recently been successfully flight tested in the IRVE-2 and IRVE-3 projects through the NASA Langley Research Center. Other future HIAD flights are in the planning and engineering stages. One advantage of an inflatable aeroshell is that the payload can use a greater portion of a launch vehicle over the traditional rigid aeroshell. This may manifest as a reduction in the size of a launch vehicle for a mission (and a possible reduction in cost) or enable a larger payload, mass or volume, on a currently existing launch vehicle. This paper will focus on a variety of mission applications of the stacked torus type attached HIAD to the Mars southern highlands, specifically landing at +4 km MOLA elevation.

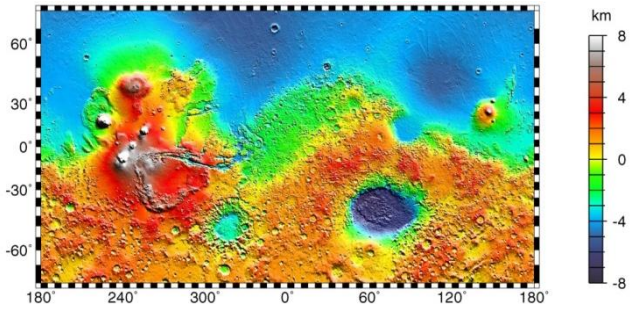

Fig. 1. Mars Elevation Map

Concept level simulation results will be shown for multiple concepts of operations (architectures) to explore the best pairing of the HIAD with secondary and possible tertiary decelerators. Decelerator options include retropropulsion and parachutes as well as examining the staging conditions. A large trade space will be examined for each architecture; the expectation is that the architectures will provide the best performance over only a portion of the trade space. Extensive early exploration of the trade space will help direct future effort to systems appropriate to a mission goal.

978-1-4673-1813-6/13/$31.00 ©2013 IEEE
[1] IEEEAC paper #2196, Version 1, Updated October 19, 2012

Error! Reference source not found. lists out the proposed architectures. The number of architectures was unknown at the beginning and descriptions were long, therefore a numbering scheme was devised to describe each architecture. The first number maps to the hypersonic regime, the second to the supersonic regime, and the third to the subsonic regime The HIAD is element 01, a supersonic retropropulsion stage is element 02, a supersonic parachute is element 03, a subsonic parachute is element 05, and a subsonic retropropulsion stage is element 06. Other elements and architectures have been proposed and eliminated or not fully analyzed due to time constraints and are not mentioned here. Architecture 01.01.05 uses a HIAD in the hypersonic and supersonic regimes and stages to a parachute subsonically. Architecture 01.01.06 uses a HIAD in the hypersonic and supersonic regimes and stages to a subsonic retropropulsion stage. Architecture 01.02.02 uses a HIAD in the hypersonic regime and stages to a supersonic retropropulsion stage that is used in the subsonic regime to touchdown. Architecture 01.03.03 uses a HIAD in the hypersonic regime and stages to a supersonic parachute that is used in the subsonic regime to touchdown. Architecture 01.03.06 uses a HIAD in the hypersonic regime, stages to a supersonic parachute, and then stages to a subsonic retropropulsion stage.

Given the uncertain future direction of the Mars program, a large range of entry masses are examined from 500 kg up to 6000 kg. This provides for a range of missions like Pathfinder up to future large robotic missions which are limited in mass by currently available launch vehicles. A range of entry velocities is examined to represent a variety of possible future launch opportunities. Other trade study parameters include entry flight path angle, HIAD diameter, parachute diameter, engine type, engine ignition velocity, and the touchdown landing system. Various constraints are applied such as an entry acceleration limit of 20 G's, TPS peak heat rates, a requirement of a minimum of 1 km in altitude for the powered flight phase, a maximum of 80% throttle, and a landed elevation of +4 km MOLA.

As proposed, and flown in IRVE-2/3, the HIAD would be inflated exoatmospheric. This cycle of the analysis has the HIAD flying hypersonically in a ballistic mode with no lift. The remainder of the EDL sequence varies with the architecture; more detail is provided in the relevant sections.

This study investigates near term HIAD technology to characterize the benefit in terms of landed mass to the surface of Mars and landing site elevation. The ability to land larger/more massive rovers to the surface of Mars means that more science instruments can be placed on those rovers, resulting in a higher mission return. The ability to land at higher site elevations opens up more of Mars's surface to exploration.

2. Models and Simulation

The Program to Optimize Simulated Trajectories II (POST2) was used in this study as the main simulation. There are a number of different models used in the simulation, which are described in the following paragraphs. Uncertainty sources for the Monte Carlos analysis are also addressed in this section.

POST2 Simulation

The POST2[3] simulation was used for the analyses, integrating the translational equations of motion. This simulation has a long heritage in previous EDL flight experience[4][5][6][7]. POST2 is a generalized point mass, discrete parameter targeting and optimization trajectory simulation program used for mission and system development support, engineering trade studies, development of reference trajectories, and mission planning and operation support at NASA Langley Research Center. POST2 has the ability to simulate three-degree-of-freedom (3DoF), 6DoF (including the rotational equations of motion), and multi-degree-of-freedom trajectories for multiple vehicles, simultaneously, in various flight regimes. POST2 also has the capability to incorporate various gravity, vehicle, propulsion, guidance, control, sensor, and navigation systems models.

Planet and Atmosphere

The POST2 simulation is using the J2-J4 gravity harmonics and the other physical parameters of Mars (planet rotation rate and radii)[8]. The atmosphere model used is Mars-GRAM 2005, which has several variables that are changed for Monte Carlo analysis. The dust tau is a seasonal

Table 1. List of Proposed Architectures.

Architecture	Hypersonic	Supersonic	Subsonic	Comments
01.01.05	HIAD	HIAD	Parachute	Small mass systems
01.01.06	HIAD	HIAD	Retroprop.	
01.02.02	HIAD	Retroprop.	Retroprop.	SRP stage to ground
01.03.03	HIAD	Parachute	Parachute	Small mass systems, large parachute
01.03.06	HIAD	Parachute	Retroprop.	MSL-like

variation based on the solar longitude. Various landing site elevations were examined in the analysis, from 0 km above the MOLA (Mars Orbiter Laser Altimeter) areoid[9] to +4 km MOLA, with the +4 km MOLA elevation results shown. The areoid is defined as a model for an equipotential surface of Mars, which is similar to sea level on Earth. Both the planetary parameters and atmospheric model have a long heritage of use in simulations supporting multiple flight projects including Mars Science Laboratory (MSL), Phoenix, and MER (Mars Exploration Rover).

Entry States

A generic B-plane state is used for these trade space analyses. This allows the entry flight path angle and entry velocity to be easily modified.

Vehicle Geometry, Mass, and Aerodynamics

The shape of the HIAD vehicle is assumed to be a 55° sphere-cone. Testing for IRVE has shown that the cone angle may change under loading but no modification is made here to account for shape distortion. The current wet entry mass of the proposed vehicles is varied from 500 kg up to 6000 kg. The HIAD Earth Atmospheric Reentry Test (HEART) aerodynamic database is used for the aerodynamics [10] and includes the same dispersions as MSL. The HIAD drag coefficient drops off quickly as the vehicle approaches and decelerates through Mach 1.

TPS Mass Model

The TPS mass model is the same as used in the Mars Entry Descent and Landing Systems Analysis (EDL-SA) [11] studies. The model itself is a calculation of areal density based on heat load. In this model, a heat rate below 20 MJ/m^2 has a constant areal density.

HIAD Mass Model

The HIAD mass modeling approach followed the EDL-SA approach [12], which provides a parametric mass model that mathematically represents mass components as a function of vehicle dimensions and key mission environmental parameters such as maximum dynamic pressure. The approach uses dimensional analysis to identify a set of dimensionless parameters for inflation pressure, mass of inflation gas, and mass of flexible material. The dimensionless parameters enable scaling of an inflatable concept with geometry parameters (e.g., diameter), environmental conditions (e.g., dynamic pressure), inflation gas properties (e.g., molecular mass), and mass growth allowance. This technique is applicable for attached (e.g., tension cone, hypercone, and stacked toroid) and trailing inflatable aerodynamic decelerators. The technique uses simple engineering approximations that were developed by NASA in the 1960s and 1970s, as well as some recent important developments. The NASA Mars EDL-SA project used this technique to estimate the masses of the inflatable concepts that were used in the analysis. The EDL-SA results compared well with two independent sets of high-fidelity finite-element analyses.

Vehicle Mass Models

The objective of the mass modeling effort was to develop a scalable, parametric mass model of the supersonic retropropulsion (SRP) stage and lander functional element (LFE) to support integrated EDL performance analysis and trades. The SRP stage includes all of the functions required for descent and terminal landing propulsion, while the LFE includes all other functions required by the integrated system at terminal landing. This functional element split is required so that the various terminal landing options could be readily traded.

The Exploration Architecture Model for IN-space and Earth-to-orbit (EXAMINE)[13] modeling framework, developed in-house at NASA Langley Research Center, was used to model the mission events and develop the parametric mass estimates of the SRP and LFE. Use of the parametric framework, as opposed to employing a more detailed design process, was deemed appropriate given the breadth of trades planned for the study effort. Specific tasks developing detailed mass models for specific technologies or design approaches (such as for airbags or crushable landings) are in-work and will be incorporated in the parametric framework as they become available. The parametric models are used to generate response surface equations (RSEs) that are incorporated directly into the flight performance (POST2) simulation. Use of this RSE methodology, demonstrated in previous EDL study efforts[11], allows an increase in analytical efficiency and utility by enabling the following:

1. Elimination of manual trajectory-sizing iterations
2. Enabling mass closure within the trajectory optimization framework
3. Enabling optimization of system configuration and element sizing variables in conjunction with trajectory optimization

Error! Reference source not found. illustrates the process and data flow for the RSE methodology. The process starts with identifying the independent (input) variables and the required upper and lower bounds. The dependent (output) variables are also identified and the integrated sizing and mass closure model is constructed to calculate these outputs as a function of the input variables. A design of experiments (DOE) driver tool built into the EXAMINE framework was used to define the DOE cases, then for each case it sets the variable inputs, executes/converges, and collects the variable outputs. Upon completion of the DOE cases, the data is fit into RSE form (and checked for quality of fit) and the series of equations are output into C code. This code then is integrated with the HIAD mass model code and compiled with the POST2 trajectory code to enable the trajectory performance analysis to utilize the complete mass

model during optimization. Converged solutions are returned to EXAMINE to verify modeling errors inherent in the RSE (due to lack of fit) are reasonably small.

SRP Mass Model Description

The primary SRP stage structure is modeled as a 2.6 m diameter aluminum-lithium (Al-Li) cylinder that supports the tank system and payload. Preliminary models and assumptions from the Exploration Feed Forward (EFF) Study[14] were used as a point of departure. This primary structure mass is estimated from a historically-based empirical curve fit[15]. Thrust structure mass is based on a historical fit accounting for stage diameter, the number of engines and the thrust load. Secondary structure mass is 5% of the primary plus thrust structure masses.

The reaction control system (RCS) has sixteen pressure-fed thrusters each producing a thrust of 444.82 N (100 lbf). Each thruster operates at a chamber pressure of 614.84 kPa (125 psia), a mixture ratio of 1.65, and an area ratio of 40 delivering an Isp of 301.3 sec. The RCS propellants are stored at 1551.32 kPa (225 psia) in two spherical graphite-wrapped aluminum tanks, one for nitrogen tetroxide (NTO) and one for monomethylhydrazine (MMH). Tank heaters and 10 layers of multi-layer insulation (MLI) provide thermal control for the tanks during interplanetary coast while a 41,368.50 kPa (6,000 psia) gaseous helium tank, constructed of graphite-wrapped aluminum, provides consumables for RCS tank pressurization.

Thermal control for SRP vehicle systems includes MLI, heaters and a heat pipe heat rejection system. Mass estimate for the SRP thermal control system (TCS) is derived from MSL. In addition, mass estimates for cabling, instrumentation and stage separation pyro-bolt mechanisms were derived from MSL.

Ground rules of the EFF study required the total mass margin be 49.5% of the basic dry mass which includes allocations for both mass growth allowance (MGA) and project managers reserve (PjMR).

In the EFF study the mission goal was to deliver 2-5 metric tons of payload to the surface of Mars using an SRP stage that provides retro-propulsion for supersonic, subsonic and terminal landing. Because the target payload and SRP delta-V for the EFF mission is substantially greater than that required for an MSL-like mission profile (that utilizes mono-propellant hydrazine engine with an Isp = 220 sec), a substantial increase in usable propellant required to land is expected. Utilizing an engine system that delivers higher specific impulse is needed to keep the SRP stage mass to a minimum. Thus, mono-propellant hydrazine was not considered for this study. Bi-propellant systems considered included the following four options:

1. Pump-fed engine burning nitrogen tetroxide (NTO) and monomethylhydrazine (MMH)
2. Pressure-fed engine burning nitrogen tetroxide (NTO) and monomethylhydrazine (MMH)
3. Pump-fed engine burning liquid oxygen (LOX) and liquid methane (CH4)
4. Pressure-fed engine burning liquid oxygen (LOX) and liquid methane (CH4)

EXAMINE's parametric engine performance and mass

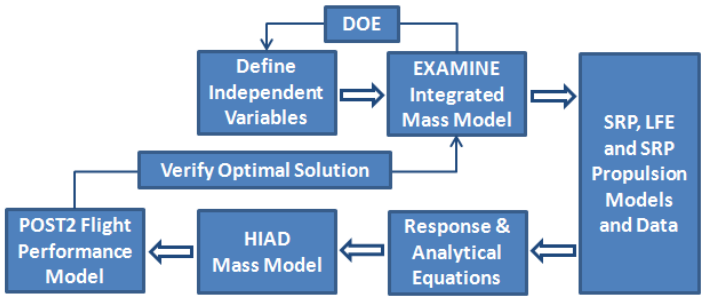

SRP RSE Independent & Dependent Variables	Lower Bound	Upper Bound
x1: Payload + LFE Mass	2 t	6 t
x2: SRP OMS Propellent Mass	100 kg	5000 kg
x3: SRP Stack Initial T/W (Mars g's)	0.5 g's	5.0 g's
x4: SRP Engine Area Ratio	100	400
y1: SRP stage dry mass (kg)		
y2: SRP stage inert mass (kg)		
y3: SRP stage initial mass (kg)		
y4: SRP thrust per engine (lbf)		
y5: SRP RCS propellant mass (kg)		
y6: SRP Ideal ΔV (m/s)		

LFE Model Independent & Dependent Variables	Lower Bound	Upper Bound
x1: Payload + SRP Mass	2 t	10 t
x2: LFE Power Required	500 W	5000 W
x3: LFE Mass Growth Allowance	0.1	0.7
x4: LFE Gear/Airbag Fraction of Landed Mass	.01	.25
y1: LFE dry mass (kg)		
y2: LFE MGA mass (kg)		
y3: LFE stage initial mass (kg)		
y4: Landed Mass (kg)		

Fig. 2. Process and Variables Used for Response Surface Methodology.

model was calibrated to known engines such as Rocketdyne's RS-72 pump-fed NTO/MMH engine[16] and the pressure-fed NTO/MMH orbital maneuvering engine (OME) used on the Space Shuttle orbiter[17]. The calibrated pump- and pressure-fed engine model was then used to extrapolate the performance and mass of the LOX/CH4 options.

As shown in Fig. 3 for the pump-fed NTO/MMH option, the engine model predicts vacuum specific impulse, engine thrust-to-weight, engine length and engine exit diameter as a function of thrust per engine, chamber pressure, mixture ratio and nozzle expansion (or area) ratio.

The engine performance and mass model, coupled with the SRP stage sizing model, was then used for a quick stage sizing comparison that compares the SRP dry and wet mass across the four propulsion configurations so that a baseline bi-propellant propulsion option could be selected for this study. The quick study uses the following common assumptions for each case:

- 3,500 kg payload plus LFE mass
- 1,500 m/s ideal delta-V for SRP main engine
- SRP engine sized to provide 3.7 Mars g's acceleration at engine start
- SRP engine area ratio equals 250
- 30 m/s for RCS attitude control during SRP maneuver
- 180 day interplanetary transfer time (for cryogenic propellant boil-off considerations)

Results of the quick stage sizing comparison is shown in **Table 2**. Note that these masses do not include the payload landed and the LFE systems.

The pump-fed NTO/MMH stage dry mass is less than half of that for the pressure-fed NTO/MMH case. This is due to the pressure-fed engine having a 1) lower engine Isp; 2) lower engine thrust-to-weight ratio; and 3) higher propellant tank storage pressure. These combined factors result in a larger usable propellant load and a stage with heavier propulsion system dry mass.

Similar trends are observed when comparing the pump-fed LO2/CH4 to the pressure-fed LO2/CH4.

Lastly, when comparing the pump-fed NTO/MMH to the pump-fed LO2/CH4 case, we see that the NTO/MMH system requires less dry and gross stage mass despite the Isp advantage of LO2/CH4. This is because the low density of the cryogenic methane fuel requires more dry mass (larger tanks and more structure to support the tankage, increased tank thermal control) and the inert mass is increased relative to the storable options due to the boil-off of the cryogenic propellants during the interplanetary coast.

Table 2. Comparison of Preliminary SRP Bi-Propellant Propulsion Options.

Engine Parameters	Pump-Fed NTO/MMH	Press-Fed NTO/MMH	Pump-Fed LO2/CH4	Press-Fed LO2/CH4
Initial Stage Thrust-to-Weight, Mars g's	3.7	3.7	3.7	3.7
Thrust per Engine, lbf (x4 Engines)	5,656	7,462	5,913	7,059
Chamber Pressure, psia	856	200	856	200
Area ratio	250	250	250	250
Mixture Ratio	2.05	1.65	3.40	3.40
Vacuum Specific Impulse, sec	336.7	325.8	370.2	368.8
Engine Thrust-to-Weight	43.1	13.8	41.1	14.7
Engine Length, m	1.60	3.87	1.65	3.72
Engine Exit Diameter, m	0.81	1.96	0.84	1.89
Stage Mass, kg	**Pump-Fed NTO/MMH**	**Press-Fed NTO/MMH**	**Pump-Fed LO2/CH4**	**Press-Fed LO2/CH4**
Dry Mass w/ Growth	**1,015**	**2,353**	**1,207**	**2,358**
Primary Body Structure	108	120	127	135
Secondary Body Structure	12	13	14	15
Space Engines & Installation	238	982	261	872
RCS Engines & Installation	75	75	75	75
Main Fuel Tanks & Feed/Fill/Drain System	78	150	106	174
Main Oxidizer Tanks & Feed/Fill/Drain System	83	148	97	178
RCS Fuel Tanks & Feed/Fill/Drain System	23	1	34	1
RCS Oxidizer Tanks & Feed/Fill/Drain System	23	1	37	2
Pressurization System	10	53	27	97
Power Distribution	5	5	5	5
Multi-Layer Insulation	10	10	10	10
Tank Heaters	5	5	5	5
Heat Pipe HRS	4	4	4	4
Pyro Bolt Separation Mechanisms	5	5	5	5
MGA + PjMR	336	779	400	781
Reserve/Residual/Press Mass	**57**	**87**	**284**	**92**
Main/RCS Press	2	13	7	28
Residual Main Fuel	18	27	12	14
Residual RCS Fuel	1	1	0	0
Boiloff Main Fuel	0	0	49	0
Residual Main Oxidizer	36	45	40	48
Residual RCS Oxidizer	1	1	1	1
Boiloff Main Oxidizer	0	0	175	0
Inert Mass	**1,072**	**2,440**	**1,491**	**2,450**
Propellant	**2,746**	**3,714**	**2,659**	**3,183**
Usable Main Fuel	876	1,365	588	705
Usable Main Oxidizer	1,796	2,252	2,001	2,396
Usable RCS Fuel	28	37	17	20
Usable RCS Oxidizer	46	61	53	63
Gross Mass	**3,818**	**6,154**	**4,150**	**5,634**

Two key issues related to risk need to be considered further:

1. Mission risk associated with starting four pump-fed engines (utilizing a gas generator cycle) for the supersonic retro-propulsion maneuver following the 6-9 month interplanetary coast from Earth to Mars.

2. Development risk to enable deep throttling of the pump-fed engine to support landing: four engines operating together require throttling to 20% power level for landing while two engines operating together (with two shutdown) require throttling to 40% power level.

This study, however, did not formally assess propulsion system risk. Future studies should carefully consider these issues.

In addition to the engine model assumptions discussed above, mass modeling for the pump-fed NTO/MMH propulsion system assumes the propellants are stored at 275.79 kPa (40 psia) in two spherical graphite-wrapped aluminum tanks, one for NTO and one for MMH. Tank heaters and 10 layers of MLI provide thermal control for the tanks during the long interplanetary coast while a 41,368.50 kPa (6000 psia) gaseous helium tank, constructed of graphite-wrapped aluminum, provides consumables for propellant tank pressurization.

The resulting model was used to generate a set of RSE's that were provided to the flight performance model. As shown in Fig. 3, several dependent variables were calculated as a function of four independent variables:

1) Payload plus LFE mass (in metric tons)

2) Usable main propellant mass (in kilograms)

3) SRP stage acceleration at SRP start (in Mars g's)

4) SRP engine area ratio

LFE Model

The landing functional element (LFE) mass model includes the common and dedicated functional subsystems for the various landing mode trade options considered. Common subsystems, regardless of the landing mode type, include batteries for power generation during landing; power management and distribution systems; guidance, command, control and data handling (CCD&H); navigation and control (GN&C); tele-communications; landing radar with antenna; and the SRP engine controller. Optional subsystems (depending on landing option) include landing legs; subsonic parachutes; crushable structures; landing airbags; and terminal landing propulsion. For year 1 activities, only the landing legs, select crushables, and airbag models were considered at this time.

For the common function subsystems, mass estimates are derived directly from MSL.

For the optional subsystems, a basic parametric approach was utilized initially while more detailed models are in development. Landing leg and airbag system masses are determined parametrically as a function of landed mass. Typical values for landing legs range from 2-5% of the landed mass, although small robotic-class landers using landing legs[18] could potentially have a higher landing leg fraction. For landing airbags, a range of 1-5% is typical. As a point of reference, a land landing study for the Orion capsule was performed[19] and the resulting landing airbag fraction was approximately 2.5%. For robotic-class missions with smaller landed mass the airbag fraction could be a higher fraction of the mass.

Parachute

The Disk-Grap-Band (DGB) parachute model is derived from the same data used by the MSL team[20]. It is capable of defining the parachute aerodynamics throughout the Mach range with dispersions. It also calculates the time to line stretch from mortar fire and the inflation time. For comparison, the DGB parachute is sized at a diameter of 21.5 m. A 23 m diameter DGB parachute was tested in the 80 x 120 foot wind tunnel at the NASA Ames National Full-Scale Aerodynamics Complex (NFAC) at subsonic conditions [2].

3. ARCHITECTURE 01.01.05/01.03.03 RESULTS

Architecture 01.01.05 uses a HIAD through the hypersonic and supersonic phases; the staging is done in the subsonic regime where the vehicle is separated from the HIAD and uses a subsonic parachute to land on the surface. Table 3 lists the variables used in the trade space and the domain of each. Since the parachute is the only other decelerator device, the upper end of the parachute diameter domain is large, larger than any used on previous Mars robotic missions. The parachute is assumed to be a DGB, the same type used on Viking, Mars Pathfinder, the Mars exploration

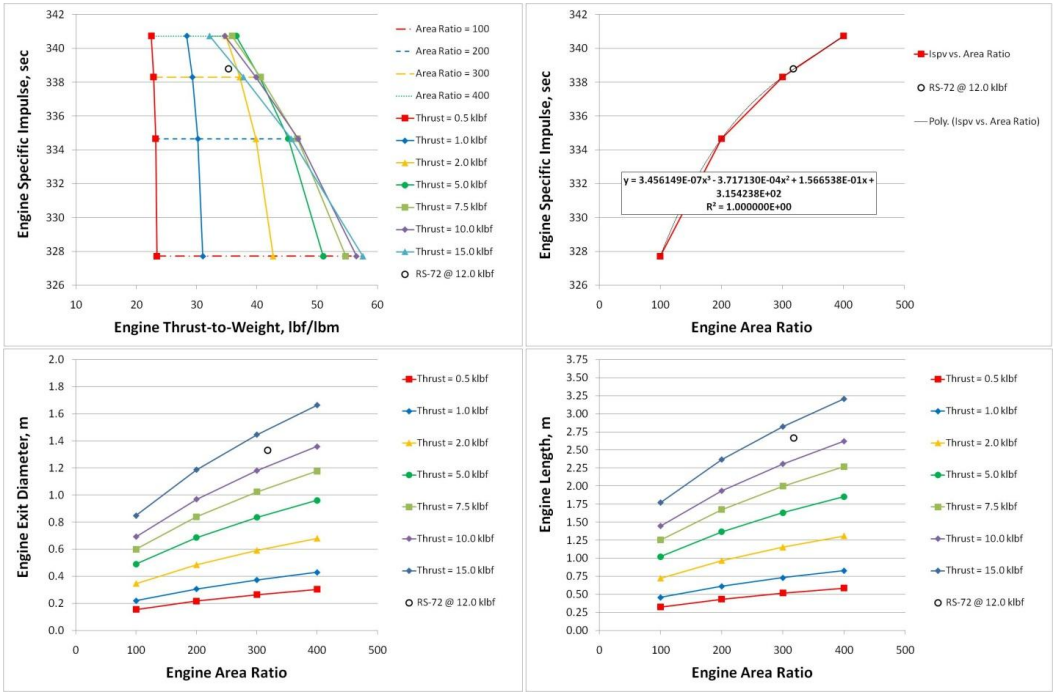

Fig. 3. Parametric Performance and Sizing Maps for a Pump-Fed NTO/MMH Rocket

rover missions, Phoenix, and MSL. The touchdown systems examined are an airbag system or a crushable material.

Table 3. Trade Space for Architecture 01.01.05.

Variable	Low Value	High Value
HIAD Diameter, m	4.0	20
Entry Mass, kg	500	6000
Entry Flight Path Angle, deg	-12	-20
Entry Velocity, m/s (hyperbolic)	3500	6000
Parachute Diameter, m	15	35
Parachute Deployment Mach	0.5	0.9

The analysis of this architecture has included a model for the landing attenuation system, either a crushable or airbag system. The airbag system model used for the current results is the first version of that model and a second version has been delivered but not yet used. The development of these models has illuminated some constraints. After consultation with experts on the landing attenuation systems, a 20 m/s landing velocity was used as a constraint. Even then, dependent on the vehicle mass at this point, that velocity may still result in an infeasible vehicle design.

A simple calculation may inform the expectation of the results for this architecture. Equation 1 is the equation for the terminal velocity of a falling vehicle, assuming only a parachute and no contribution from the entry vehicle. This can be used to estimate the maximum mass that can be suspended from a 30 m diameter parachute and achieve the 20 m/s terminal velocity at +4 km MOLA elevation. Assuming a drag coefficient of 1.4 for the DGB parachute and an atmospheric density of 0.01 kg/m^3, the result is approximately 540 kg which is the low end of the trade space. Therefore, the expectation is that there will be few cases achieving the desired terminal velocity.

$$V = \left\{ \frac{2mg}{[\rho C_{D0} S_0]} \right\}^{\frac{1}{2}}$$

Equation 1. Terminal Velocity Equation.

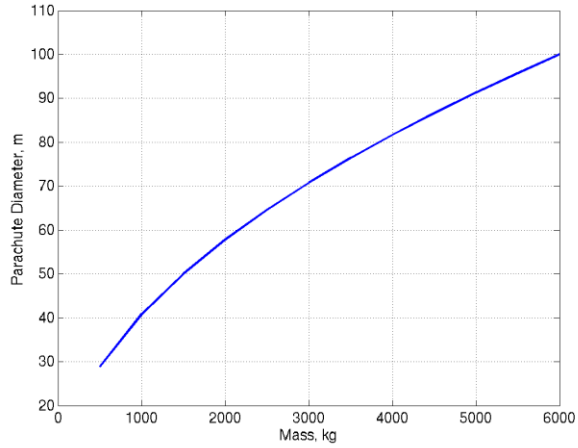

Fig. 4. Terminal Velocity at +4 km MOLA Elevation.

Fig. 4 shows the trend over a range of vehicle masses. These parachutes are all extremely large and beyond the near term parachute technology assumption. A cluster of large parachutes could be considered but may quickly become mass prohibitive; this solution is not examined in this paper.

Fig. 5 reports the HIAD diameter chosen to achieve the maximum landed mass and the corresponding landed mass. At this point, while the landed mass results are without reference to either landing attenuation system model, it appears that the architecture may be feasible for small masses. However, once either of the landing attenuation system models is incorporated into the results, there are no feasible vehicle designs left in the trade space.

There are multiple reasons for the failures; there are limits on the vehicles that are decelerated to the 20 m/s upper velocity limit with just a DGB parachute, there is a limit to the maximum stroke on either landing attenuation system, and there are limits to the crush load for the crushable system. One example is a design where the limits are not exceeded except for the stroke length; in this case the length leads to a tumble risk where the height of the crushable is greater than the other dimensions causing a possibly unstable touchdown situation.

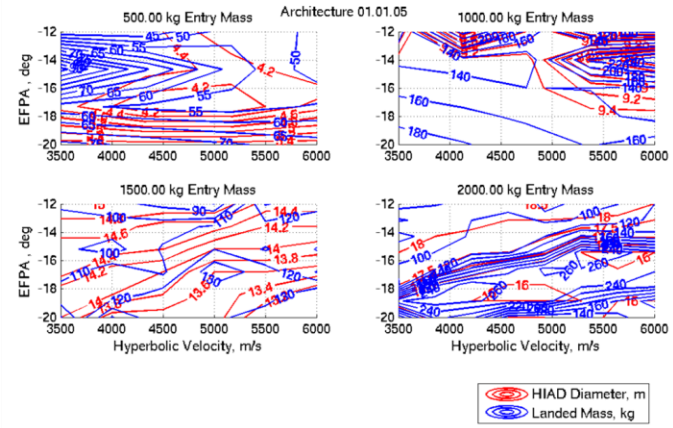

Fig. 5. Landed Mass and HIAD Diameter Results for Architecture 01.01.05.

Architecture 01.03.03 is very similar in that a parachute alone is used to decelerate the vehicle to touchdown, the only difference being that the parachute would be deploy in the supersonic regime. Since the results of architecture 01.05.05, architecture 01.03.03 was not pursued as similar results would be expected. The architecture is complicated by the supersonic deployment of the parachute since opening loads would be very large for the diameter required to decelerate the vehicle to a successful touchdown. A possible mitigation for this, reefing, is not examined in this analysis cycle.

Additionally, other additions such as small retrorockets added to the vehicle to provide a small velocity change near the surface, similar to the backshell rockets on Mars Pathfinder [21] or MER [22], were discussed but not examined in this analysis cycle.

4. Architecture 01.01.06 Results

This architecture uses a HIAD through the hypersonic and supersonic phases; the staging is done in the subsonic regime where the vehicle is separated from the HIAD and uses retropropulsion to land on the surface. Table 4 lists the variables used in the trade space and the domain of each. An additional assumption used here pertains to the subsonic retropropulsion system; a landing velocity of 2.5 m/s, which is based off of Phoenix, a throttle maximum of 80%, and a minimum of 1 km of altitude for powered descent are assumed. The powered descent is assumed to be a gravity turn without additional phase such as those introduced for the Mars Science Laboratory powered descent. All the results shown here are based on a nominal analysis with constraints applied.

Table 4. Trade Space for Architecture 01.01.06.

Variable	Low Value	High Value
HIAD Diameter, m	4.0	30
Entry Mass, kg	1000	6000
Entry Flight Path Angle, deg	-12	-20
Entry Velocity, m/s (hyperbolic)	3500	6000
Engine Ignition Mach	0.3	0.9

Multiple engine types were assessed through the propulsion and vehicle mass models. For this architecture, the pump-fed NTO/MMH bipropellant propulsion system resulted in the largest payload masses.

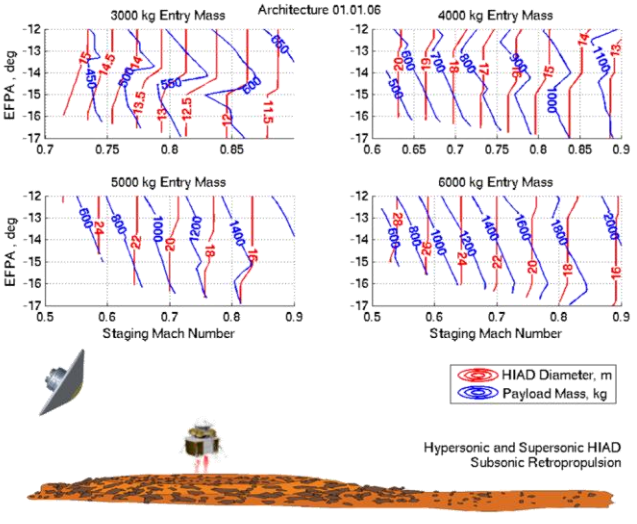

Fig. 6. HIAD Diameter and Payload Mass Results for Architecture 01.01.06.

In Fig. 6, the trade space is not fully filled with viable solutions. The various constraints become active in the different regions; for instance the 20 G entry deceleration limit is active along the bottom, the steeper entry flight path angles (EFPA), while the 80% maximum throttle setting is active along the side for the lower velocity staging conditions. Note that the necessary HIAD diameter increases rapidly as the staging Mach number decreases; the payload mass also falls rapidly since the HIAD has become a larger portion of the total vehicle mass. The drag coefficient of the HIAD decreases rapidly around Mach 1 and below, which makes the staging condition Mach number a primary driver of the HIAD diameter in this architecture.

The payload mass is zero for the 1000 kg entry mass due to mass model non-convergence. The powered descent altitude constraint eliminates the 2000 kg entry mass as a feasible solution; the HIAD mass constrains the allowable HIAD diameter which, in turn, limits the altitude for the ignition of the retropropulsion. Future improvements to the various mass models may partially alleviate the restriction if components masses and margins are able to be reduced, allowing for HIAD use on less massive vehicles.

A perceived benefit of this architecture is the elimination of supersonic deployment events.

5. Architecture 01.02.02 Results

This architecture uses a HIAD through the hypersonic phase and into the supersonic phase; the staging is done in the supersonic regime where the vehicle is separated from the HIAD and uses a retropropulsion system, from supersonic through subsonic, to land on the surface. Table 5 lists the variables used in the trade space and the domain of each. An additional assumption used here pertains to the retropropulsion system; a landing velocity of 2.5 m/s, which is based off of the Phoenix powered descent, a throttle maximum of 80%, and a minimum of 1 km of altitude for powered descent are assumed. The powered descent is assumed to be a gravity turn without additional phase such as those introduced for the Mars Science Laboratory powered descent.

Table 5. Trade Space for Architecture 01.02.02.

Variable	Low Value	High Value
HIAD Diameter, m	4.0	30
Entry Mass, kg	1000	6000
Entry Flight Path Angle, deg	-12	-20
Entry Velocity, m/s (hyperbolic)	3500	6000
Engine Ignition Mach	1	3

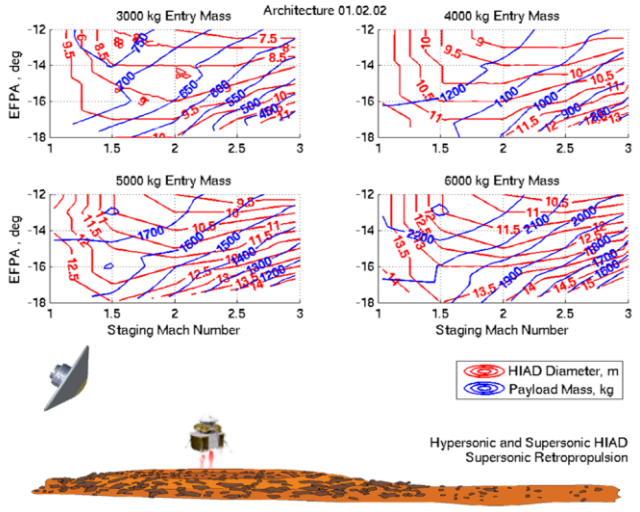

Fig. 7. HIAD Diameter and Payload Mass Results for Architecture 01.02.02.

Fig. 7 shows the results for the HIAD diameter chosen to produce the maximum payload mass subject to all the constraints previously listed. The largest difference with Architecture 01.01.06 is the smaller resulting HIAD sizes; this is explained by the fact that the staging conditions here are supersonic. Per the discussion of the HIAD drag coefficient in the results section of Architecture 01.01.06, the drag coefficient decreases with the Mach number and rapidly so around Mach 1 and below. This also explains the turning of the diameter contours as the staging Mach number approaches one. The trend towards a larger HIAD in the lower right corners of each contour plot is mainly driven by the EFPA and throttle setting. As the EFPA steepens, the altitude at the staging condition, given a constant diameter vehicle, will decrease. At some point the altitude is such that the maximum throttle setting comes against the limit, an 80% maximum in this study. In response, the HIAD diameter increases to gain altitude for the steep EFPA cases which allow a throttle setting at or below the maximum. This sensitivity would change for a powered descent assumption different from the gravity turn assumed here.

6. Architecture 01.03.06 Results

This architecture uses a HIAD through the hypersonic regime and stages to a supersonic parachute and then stages again to subsonic retropropulsion to land on the surface. Table 6 lists the variables used in the trade space and the domain of each. An additional assumption used here pertains to the subsonic retropropulsion system; a landing velocity of 2.5 m/s, which is based off of Phoenix, a throttle maximum of 80%, and a minimum of 1 km of altitude for powered descent are assumed. The powered descent is assumed to be a gravity turn without additional phase such as those introduced for the Mars Science Laboratory powered descent.

Table 6. Trade Space for Architecture 01.03.06.

Variable	Low Value	High Value
HIAD Diameter, m	4.0	30
Entry Mass, kg	1000	6000
Entry Flight Path Angle, deg	-12	-20
Entry Velocity, m/s (hyperbolic)	3500	6000
Engine Ignition Mach	0.3	0.9
Parachute Deployment Mach	1.0	2.0
Parachute Diameter, m	15	30

Multiple engine types were assessed through the propulsion and vehicle mass models. For this architecture, the pump-fed NTO/MMH bipropellant propulsion system resulted in the largest payload masses.

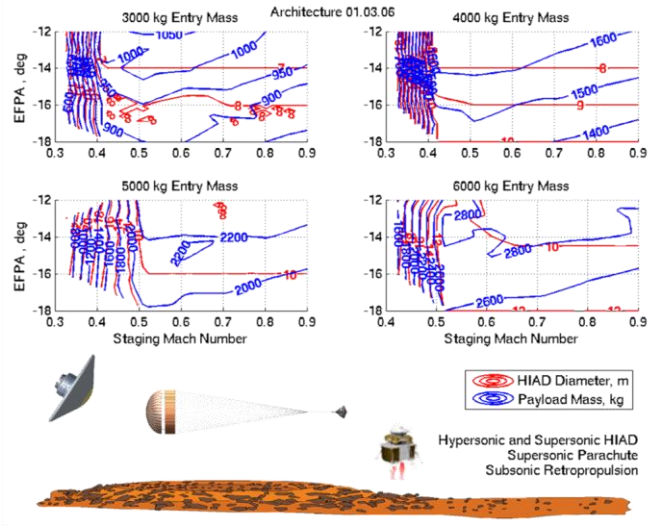

Fig. 8. HIAD Diameter and Payload Mass Results for Architecture 01.03.06.

The staging Mach number in Fig. 8 refers to the engine ignition condition. The contours become vertical around Mach 0.4-0.5; this is the point where the vehicle mass is forced to decrease due to the capability of the parachute. At some point the parachute can no longer decelerate the vehicle unless the vehicle is lighter; the lower the desired staging Mach condition, the lower the mass. This applies assuming that the parachute diameter can no longer increase; this trade space analysis limits the parachute size to 30 meters in diameter.

7. Additional Considerations/Discussion

HIAD Separation

At some point during the EDL sequence, the HIAD needs to be successfully separated from the rest of the vehicle which continues to the surface. For the supersonic retropropulsion architectures, the method assumed for this study is to separate the heatshield and HIAD in the supersonic regime allowing the descent stage, with payload, to ignite its engines in the supersonic flow. The same method is used for the subsonic separations as well. The ballistic coefficient difference between the vehicle with the HIAD and the rigid

heatshield, basically just a nosecap, will need to be large enough to ensure positive separation, in the same way as previous missions. The HIAD separation itself is expected to be quick as the HIAD will have a low ballistic coefficient and the descent stage will be much more compact with less aerodynamic surface with a larger mass making for a much higher ballistic coefficient. The mismatches will be dependent on the particular vehicle design from the large trade space. This study has not examined this concept of operations in any depth in terms of mechanisms. Future studies will need to address these events since a separation event is always a concern to a mission, especially a supersonic separation.

HIAD Deceleration to Low Velocities

Multiple architectures examined the use of a HIAD to decelerate a vehicle down to low supersonic or subsonic velocities. One motivation is to relieve the perceived risk of supersonic deployment events and phenomenon like parachute area oscillations that are expected at Mach numbers approximately above Mach 1.5[23]. To achieve this deceleration, a large HIAD is required for the high entry masses. Future additions to the transonic and subsonic data, shown in Fig. 9, are needed to better characterize the vehicle since this an important region for multiple architectures.

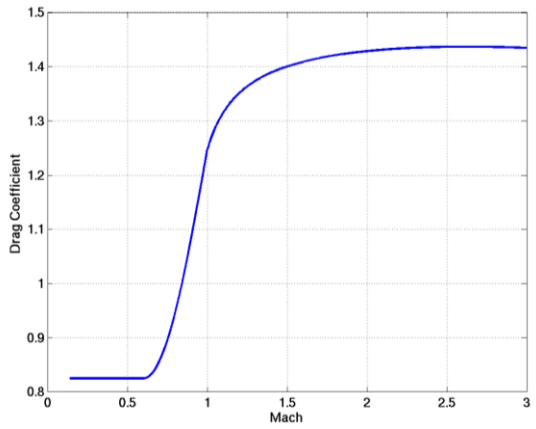

Fig. 9. Transonic and Subsonic Drag Coefficient.

If the drag coefficient were increased in light of new data, the HIAD diameters required to achieve subsonic deceleration would decrease which would have the overall effect of increasing the payload to the surface.

Extensibility

HIADs are perceived to be extensible from MSL class missions to large robotic missions and human precursor missions and even up to human scale missions[11]. At the human scale, other aerodynamic decelerators such as parachutes, become less useful and staging from a HIAD to retropropulsion becomes more attractive.

Future Studies

Future studies should update models based on new data, especially mass models. For smaller mass vehicles, the addition of another decelerator such as retropropulsion, similar to Pathfinder, to the subsonic parachute architectures, 01.01.05 and 01.03.03, may enable those concepts to close. A packaging study would also be recommended. Again, all the results shown here are based on a nominal analysis with constraints applied. Performance parameters such as pinpoint landing or divert capability may be a discriminator between architectures.

8. CONCLUSIONS

The use of a HIAD for a Mars mission has been shown to be an effective means of decelerating a vehicle, for a range of entry masses, to supersonic or subsonic staging conditions. Selecting an architecture may be mission specific and depend on the mission risk posture, technology goals, and performance goals like payload to the surface and landed elevation/surface access.

Near term missions may use architecture 01.03.06 to achieve comparatively higher payload masses to the surface, while the vehicle masses are within the current and foreseeable parachute capability. Other missions may select architecture 01.01.06 to eliminate any supersonic deployment and separation events. Architecture 01.02.02 could serve as a technology demonstration mission for supersonic retropropulsion; this architecture is also extensible to larger robotic and human scale missions.

9. ACKNOWLEDGEMENTS

The research was managed by the National Aeronautics and Space Administration Langley Research. The research was a joint effort by NASA Langley Research Center, Analytical Mechanics Associates, and Binera Inc.

REFERENCES

[1] M. S. S. Systems. (2006, Dec.) New Gully Deposit in a Crater in Terra Sirenum: Evidence That Water Flowed on Mars in This Decade?. [Online]. http://www.msss.com/mars_images/moc/2006/12/06/gullies/sirenum_crater/index.html

[2] D. S. Adams and N. P. Onufer, "Mars Science Laboratory Parachute Development Test Program," 21st AIAA Aerodynamic Decelerator Systems Technology Conference and Seminar , AIAA 2011-2508, 2011.

[3] G. L. Brauer, D. E. Cornick, and R. Stevenson, "Capabilities and Applications of

the Program to Optimize Simulated Trajectories (POST)," Martin Marietta Corporation NASA CR-2770, 1977.

[4] J. L. Davis, A. Dwyer Cianciolo, R. W. Powell, J. D. Shidner, and E. García-Llama, "Guidance and Control Algorithms for the Mars Entry, Descent and Landing Systems Analysis," AIAA Astrodynamics Specialist Conference , AIAA-2010-7972, 2010.

[5] S. A. Striepe, D. W. Way, A. M. Dwyer, and J. Balaram, "Mars Smart Lander Simulations for Entry, Descent, and Landing," AIAA Atmospheric Flight Mechanics Conference and Exhibit , AIAA-2002-4412, 2002.

[6] P. Desai, M. Schoenenberger, and F. M. Cheatwood, "Mars Exploration Rover Six-Degree-of-Freedom Entry Trajectory," *Journal of Spacecraft and Rockets*, vol. 43, no. 5, pp. 1019-1025, Sep. 2006.

[7] J. L. Prince, P. N. Desai, E. M. Queen, and M. R. Grover, "Mars Phoenix Entry, Descent, and Landing Simulation Design and Modeling Analysis," AIAA/AAS Astrodynamics Specialist Conference and Exhibit , AIAA 2008-7507, 2008.

[8] "Mars Science Laboratory Planetary Constants and Models Document," JPL D-27212, 2008.

[9] G. A. Neumann, F. G. Lemoine, D. E. Smith, and M. T. Zuber, "The Mars Orbiter Laser Altimeter Archive: Final Precision Experiment Data Record Release and Status of Radiometry," Proceedings of the 34th Lunar and Planetary Science Conference, 2003.

[10] M. Schoenenberger, A. Dyakonov, P. Buning, W. Scallion, and J. Van Norman, "Aerodynamic Challenges for the Mars Science Laboratory Entry, Descent and Landing," 41st AIAA Thermophysics Conference , AIAA 2009-3914, 2009.

[11] A. Dwyer Cianciolo, et al., "Entry, Descent and Landing Systems Analysis Study: Phase 1 Report," NASA Langley Research Center TM-2010-216720, 2010.

[12] J. A. Samareh, "Estimating Mass of Inflatable Aerodynamic Decelerators Using Dimensionless Parameters," in *8th International Planetary Probe Workshop*, Portsmouth, VA, 2011.

[13] D. R. Komar, J. Hoffman, A. Olds, and M. Seal, "Framework for the Parametric System Modeling of Space Exploration Architectures," in *AIAA SPACE 2008 Conference & Exposition*, San Diego, CA, 2008.

[14] A. Dwyer Cianciolo, et al., "Entry, Descent and Landing Systems Analysis Study: Phase 2 Report on Exploration Feed-Forward Systems," NASA Langley Research Center TM-2011-217055, 2011.

[15] W. Heinemann, "Design Mass Properties II: Mass Estimating and Forecasting for Aerospace Vehicles Based on Historical Data," JSC JSC-26098, 1994.

[16] A. S. &. Technology. (2001) RS-72 - Specifications. [Online]. http://www.spaceandtech.com/spacedata/engines/rs72_specs.shtml

[17] M. Wade. Encyclopedia Astronautica OME.

[18] N. A. a. S. Administration, "Phoenix Landing: Mission to the Martian Polar North," National Aeronautics and Space Administration Press Kit, 2008.

[19] B. Tutt, C. Sandy, and J. Corliss, "Status of the Development of an Airbag Landing System for the Orion Crew Module," in *20th AIAA Aerodynamic Decelerator Systems Technology Conference and Seminar*, Seattle, WA, 2009.

[20] J. Cruz, "Mars Science Laboratory Supersonic Parachute Data," 2003.

[21] M. P. Golombek, "The Mars Pathfinder Mission," *Journal of Geophysical Research*, vol. 102, no. E2, pp. 3953-3965, Feb. 1997.

[22] NASA, "Mars Exploration Rover Landings," NASA Press Kit, 2004.

[23] A. Witkowski, M. Kandis, and D. S. Adams, "Inflation Characteristics of the MSL Disk Gap Band Parachute," in *20th AIAA Aerodynamic Decelerator System Technology Conference and Seminar*, Seattle, WA, 2009.

BIOGRAPHIES

Richard Winski *is an aerospace engineer at Binera, Inc. in the Atmospheric Flight and Entry Systems Branch at NASA Langley. He received a B.S. in Aerospace Engineering from the Virginia Polytechnic Institute and State University(Virginia Tech) in 2004 and M.S. in 2006 through Virginia Tech and the National Institute of Aerospace (NIA). While completing his M.S. he worked in the Atmospheric Flight and Entry Systems Branch at NASA Langley. His current work is in the area of flight dynamics and simulation for Entry, Descent and Landing (EDL).*

Dave Bose i*s an aerospace engineer for Analytical Mechanics Associates.*

David R. Komar *is an aerospace engineer in the Vehicle Analysis Brach at NASA Langley Research Center.*

Jamshid Samareh *is an aerospace engineer in the Vehicle Analysis Brach at NASA Langley Research Center.*